Copy 26
RM SL54C03

NACA

RESEARCH MEMORANDUM

for the

U. S. Army Ordnance

PRELIMINARY FLIGHT MEASUREMENTS OF THE TOTAL-PRESSURE RECOVERY OF A SPLIT-WING RAM-JET INLET AT MACH NUMBERS FROM 1.4 TO 3.16

By Arthur H. Hinners, Jr.

Langley Aeronautical Laboratory
Langley Field, Va.

NATIONAL ADVISORY COMMITTEE
FOR AERONAUTICS

WASHINGTON

MAR 4 1954

NACA RM SL54C03

NATIONAL ADVISORY COMMITTEE FOR AERONAUTICS

RESEARCH MEMORANDUM

for the

U. S. Army Ordnance

PRELIMINARY FLIGHT MEASUREMENTS OF THE TOTAL-PRESSURE RECOVERY OF A SPLIT-WING RAM-JET INLET AT MACH NUMBERS FROM 1.4 TO 3.16

By Arthur H. Hinners, Jr.

SUMMARY

Flight tests were made to determine the total-pressure recovery of a split-wing ram-jet inlet with a fixed area exit 20 percent larger than the inlet throat over a Mach number range from 1.4 to 3.16.

Total-pressure-recovery measurements at the diffuser exit station indicated abrupt pressure changes in the total-pressure profile throughout the Mach number range. A total-pressure recovery of 0.33 was obtained at a free-stream Mach number of 3.12 for 0° angle of attack. A test of a model simulating an angle of attack of -3° indicated a total-pressure recovery of 0.37 at a Mach number of 3.16.

Comparisons of average total-pressure recovery with the theoretical total-pressure recovery showed good agreement. However, the preliminary nature of the test does not allow a conclusion concerning the maximum total-pressure recovery that this inlet could attain.

INTRODUCTION

A preliminary investigation of the diffusion characteristics of a two-dimensional split-wing ram-jet inlet was conducted at the Langley Pilotless Aircraft Research Station at Wallops Island, Va., at the request of the Guided Missile Development Division of the U. S. Army Ordnance Corps in conjunction with the Hermes project. The investigation was made by mounting the inlet on a rocket test vehicle and booster; the resulting rocket combination was then able to propel the test vehicle to a maximum Mach number of approximately 3.16.

The purpose of the investigation was to determine the total-pressure recovery and internal flow characteristics of the design at 0° and -3° angle of attack, operating with a fixed area exit which gave a diffuser-exit Mach number of approximately 0.19, over a range of supersonic Mach number and Reynolds number.

Data are presented for both accelerating and decelerating flight over a Mach number range from 1.40 to 3.16 and a Reynolds number range from 5×10^6 to 17×10^6 based upon the unit "foot."

SYMBOLS

A_{cowl}	inlet capture area defined by inlet lips, sq ft
A_{cr}	choking area, sq ft
A_e	entrance area to inlet defined along imaginary surface, perpendicular to wedge surface from leading edge of inlet lip, sq ft
A_{min}	minimum area at inlet throat, sq ft
H	total pressure, lb/sq ft
m	measured mass flow through duct, slugs/sec
m_0	mass flow through a stream tube of area equal to inlet capture area under free-stream conditions, slugs/sec
M	Mach number
p	static pressure, lb/sq ft
R	gas constant, 53.3 ft/°R
S	static orifice
T	static temperature, °R
V	velocity, ft/sec
ρ	density, slugs/cu ft
x	local distance, in.
X	total distance across station 6, in.

Subscripts:

0	free-stream station
1	static orifice location on 15° portion of center-body wedge
2	static orifice location on 10° portion of center-body wedge
3	static orifice location on downstream portion of center-body wedge
4	total-pressure measuring station downstream of inlet maximum area
5	static orifice location on outer shell wall at downstream portion of subsonic diffuser
6	diffuser exit station
7	exit choking station $(M_7 = 1.00)$
l	local

MODELS AND APPARATUS

A photograph of the split-wing inlet mounted on a rocket test vehicle with booster in the launching altitude is presented in figure 1. Photographs of the three inlet models tested and a detailed diagram are shown in figures 2 and 3, respectively.

The inlet consists of an outer wall and a wedge inner body that makes the configuration essentially a split-wing inlet. The opposite side of the test inlet serves only to make the flight test vehicle symmetrical. A plate connects the inner-body wedge and the downstream mounting base in order to make the two ducts separate and distinct. Models A and B were of the same design but had pressure rakes and orifices located at different stations as indicated on figure 3.

The leading edge of models A and B had an initial angle of 20° which was turned by finite corners progressively to 15°, 10°, and 0°, and was diffused in the subsonic portion of the inlet with an included angle of 6°. Near the end of the subsonic diffuser, both the wedge and the outer shell turned outward through an abrupt radius to the diffuser exit. The passage then converged to a choking exit station having an area 20 percent greater than the inlet minimum station. The flow exited through a side passage. Model measurements at final assembly showed models A and B

to have small dimensional differences as indicated in figure 3. The lip leading edge of model A was located 1.56 inches downstream of the leading wedge and 1.11 inches from the model center line; the lip leading edge of model B was located 1.54 inches downstream of the leading wedge and 1.10 inches from the center line. Both model A and model B had a contraction ratio A_{cowl}/A_{min} of 0.36, an exit height at station 7 of 0.48 inch, and an internal width of 4.00 inches.

Model C simulated models A and B at -3° angle of attack by reducing the leading wedge angle from 20° to 17°. The inner surface of the lip was also turned 3°. As a result, the leading wedge had finite corners which turned progressively from 17° to 12°, 7°, and -3°, and diffused in the subsonic portion with an included angle of 6°. As in the other models, the diffuser exit was 1.50 inches in height. Model C had a choking-exit-station height of 0.47 inch, and a contraction ratio A_{cowl}/A_{min} of 0.40. The lip leading edge was located 1.58 inches downstream of the wedge leading edge and was 1.00 inch from the model center line. The inlets were constructed of steel and all leading edges were machined to knife edges. All surfaces were polished smooth and fair. At final assembly a small silver solder fillet was soldered in all corners of the inlet lips.

INSTRUMENTATION

Each model was equipped with a telemetering system which transmitted eight channels of information continuously. Six channels of information of each model were used for inlet internal pressures and two channels were used to transmit the model longitudinal acceleration. The six locations of the measured internal pressure for each model can be seen in figure 3. Models A and C had four total-pressure tubes and two wall static orifices located at station 6. Two static orifices were also located at stations 3 and 5. Model B had two total-pressure tubes at station 4 and two total-pressure tubes and two static orifices at station 7, the exit station. Also, two static orifices were located at stations 1 and 2, portions of the inner-body wedge where the angle was 15° and 10°, respectively. In order to reduce the range of the pressure measuring cells, the differential pressure was measured between each total-pressure tube and the nearest wall static orifice. This differential pressure was then added to the recorded static-pressure measurement to obtain the total pressure.

A CW Doppler radar unit was used for obtaining the model velocity. However, the CW Doppler radar lost model B during the sustainer firing portion of the flight, and the velocity and Mach number for the rest of the flight were determined by integrating the accelerometer record. All velocities were corrected for winds aloft. AN NACA modified SCR 584 tracking radar set was employed to obtain the model range, elevation,

[redacted]

and azimuth as a function of time. Atmospheric conditions were determined from a radiosonde released at the time of firings. Fixed and manually operated 16-millimeter and 70-millimeter cameras were employed to record the launching and initial portion of the flight tests.

TESTS AND ANALYSIS

Tests

All model-booster combinations were launched at an elevation angle of 60° from a mobile-type launcher as shown in figure 1. The models were boosted to an approximate Mach number of 1.3 by a single 6.25-inch solid-fuel ABL Deacon rocket motor. The sustainer rocket of model A was timed to fire at booster burnout time and was further accelerated to a peak Mach number of 3.16 where inlet failure occurred and no further data were obtained. In order to alleviate the aerodynamic forces at the maximum Mach number, models B and C were allowed to coast after booster burnout for approximately 12.5 seconds before the sustainer rocket fired. As a result, the altitude gained during the coasting stage allowed the maximum Mach number of approximately 3.15 and 3.16 of models B and C, respectively, to occur with lower dynamic forces, and the inlets did not fail. Data, therefore, were obtained during both accelerating and decelerating flight for models B and C.

Reynolds numbers per foot for the three models are shown in figure 4 as a function of the flight Mach number. Because of the previously discussed sustainer-firing delay, the Reynolds numbers per foot for models B and C are similar in value and lower for a given Mach number than model A. Progressive time is indicated by arrows to differentiate between accelerating and decelerating portions of the flights.

Although the models were symmetrical about the longitudinal axis, the models did experience roll and this quantity is shown in figure 5 as the rate of roll as a function of the flight Mach number.

Calculations of the induced angle of attack due to roll indicate a maximum induced angle at the outer edge of the inlet wedge of less than 0.07° over the entire Mach number range. The roll effect on inlet performance is, therefore, considered insignificant.

Analysis

The position of the models in space was determined by the tracking radar set. Free-stream static pressure, static temperature, and speed of sound were determined from the radiosonde data. Velocity was determined

by Doppler radar and, in the case of model B, by Doppler radar and integration of the accelerometer data. Hence, from these values the free-stream Mach number and total pressure were determined.

The average total pressure at station 6 in models A and C was found by arithmetically averaging the total pressures of the individual total-pressure tubes at these stations.

The mass flow was evaluated from the test of model B by the expression

$$\frac{m}{m_0} = \frac{H_7}{H_0} \times \frac{A_7}{A_{cowl}} \times \frac{A_0}{A_{cr}}$$

which was derived from continuity considerations by assuming $M_7 = 1.00$. The ratio H_7/H_0 was measured in model B. However, reliable data were obtained with only one (tube C) of the two total-pressure tubes at station 7. A uniform profile was assumed at station 7 and the recovery of H_c/H_0 of station 7 was used to calculate the mass-flow ratio. The ratio A_7/A_{cowl} is a geometric area ratio of the model. The ratio A_0/A_{cr} is a function of the free-stream Mach number.

The theoretical mass-flow ratio was determined by the same equation but was evaluated at the inlet throat as

$$\frac{m}{m_0} = \frac{H_2}{H_0} \frac{A_{min}}{A_{cowl}} \frac{A_0}{A_{cr}}$$

where H_2/H_0 is the total-pressure ratio across an oblique shock and a normal shock at the inlet entrance.

Accuracy

Possible systematic errors in the absolute level of directly measured quantities are proportional to the total range of the measuring instruments. On the basis of statistical data compiled by the Instrument Research Division of the Langley Aeronautical Laboratory, it is believed that the instrumentation of these models is accurate to within ± 1 percent of the full-scale range for pressure measuring instruments and $\pm 1\frac{1}{2}$ percent for the remaining instruments. Because of the necessary pressure range of the measuring instruments for the highest Mach numbers

encountered, the percentage accuracy decreased with decreasing values of Mach number. Tubing diameter and length used to connect the cells to the pressure measuring stations were selected to keep the lag in pressure measurement within the previously stated ±1 percent possible error at the time of greatest rate of change of pressure. Further possible error results from possible inaccuracies in determination of atmospheric properties and model space position.

If it is assumed that the atmospheric conditions encountered by the models are the same as those determined by the radiosonde, the following maximum errors in the absolute quantities were computed at two values of M_0:

For $M_0 = 3.15$

M_0	±0.015
H_6/H_0	±0.015
m/m_0	±0.05
p/p_0	±0.2

For $M_0 = 2.5$

M_0	±0.014
H_6/H_0	±0.03
m/m_0	±0.04
p/p_0	±0.2

Practical experience has shown that, normally, experimental errors are generally less than the maximum values of error such as those listed.

RESULTS AND DISCUSSION

All the inlet models tested had a contraction from the inlet lip to the throat station and, as a result, a normal shock was held outside the inlet lip. In order to find if the normal shock could enter the inlet at any value of Mach number reached in the tests, theoretical one-dimensional-flow calculations were made by neglecting side effects and boundary-layer buildup. The calculations indicate that the normal shock could enter the inlet of model A at $M_0 \approx 3.43$, model B at $M_0 \approx 3.35$, and model C at $M_0 \approx 3.17$. Inlet models A and B, therefore, operated with the normal shock in front of the inlet lip throughout the range of these tests, and the starting Mach number of model C was just reached at the maximum Mach number of the tests. Model C allowed the inlet to

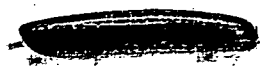

swallow the shock at a lower value of free-stream Mach number than models A and B because simulating a -3° angle of attack reduces the amount of contraction as well as increasing the strength of the normal shock at the entrance to the inlet.

Measured mass-flow ratio as a function of the free-stream Mach number is presented in figure 6 for model B, where the total pressure was measured at the exit station. Good agreement is noted with the theoretical mass flow computed by assuming choking flow at the inlet throat.

Local total-pressure recovery at station 6 in models A and C and stations 4 and 7 in model B is presented in figure 7 as a function of the free-stream Mach number.

Measurements at station 6 in models A and C show erratic breaks in the total-pressure level of the individual tubes. Similar data were obtained at stations 4 and 7 in model B. Data obtained for two of the tubes of model B were not presented as they were not considered reliable, because of some mechanical difficulty within the recording cells. The data of model C simulating -3° angle of attack appear to be more erratic than the 0° model data with many abrupt changes in the total-pressure level.

Total-pressure profiles of models A and C are presented in figure 8 for several free-stream Mach numbers. A dashed line connects the static pressure that was measured by wall static orifices; it is assumed that the static pressure varied linearly across the station.

The total-pressure tubes were differentially connected to the wall static orifices. Zero or negative differential pressures, therefore, indicate low-energy areas or wakes. Generally, the profiles of model A show there was a low-energy region behind the inner-body wedge for most of the flight Mach number range. At the higher values of Mach number, M_0 = 3.0 and 3.1, there are regions of total-pressure recovery that are lower than the measured static-pressure ratio, thus indicating a region of reverse flow. The profiles of model C are similar to those of model A except that, for an appreciable part of the Mach number range, a flow change occurred and resulted in separation off the outer wall. Comparisons of profile shapes at the same value of free-stream Mach number of model C accelerating and decelerating show in some instances different results. The normal shock may have entered the inlet minimum area near the peak Mach number and could have been retained within the inlet for part of the decelerating flight. This change in shock location could account for the differences in the profile shapes at M_0 = 3.0 and 3.1. However, the reasons for the differences in the profile shapes below these values of free-stream Mach number are not obvious.

[redacted]

Average total-pressure recovery as a function of the free-stream Mach number is presented in figure 9 for models A and C. Local total-pressure recoveries of model A accelerating were averaged and the local total-pressure-recovery averages of model C accelerating and decelerating were further averaged together. Insufficient data prevent presenting an average total-pressure recovery of model B. Theoretical pressure-recovery points for model A were determined by

$$\frac{H_6}{H_0} = \frac{H_2}{H_0} \times \frac{A_{min}}{A_7}$$

where H_2/H_0 is the theoretical total-pressure recovery across an oblique shock with a 5° corner expansion before a normal shock on the 15° surface. Then $A_{min} = A_{cr}$ since the normal shock never entered the inlet.

The reported average total-pressure recoveries might be different from those that actually exist because of boundary-layer buildup on all four walls of the diffuser and the inability of the limited instrumentation to weigh in corner and wall-boundary-layer losses.

Model A had an average total-pressure recovery of 0.33 at $M_0 = 3.12$, representing 87 percent of the theoretical total-pressure recovery. Below this value of Mach number the data more closely approach the theoretical values. Generally, the data indicate the average total-pressure recovery of this inlet with a fixed exit area 20 percent larger than the inlet throat showed good agreement with the theoretical total-pressure recovery for the entire range of free-stream Mach number. However, the preliminary nature of this test does not allow a conclusion concerning the maximum total-pressure recovery that this inlet could attain.

Model C simulating -3° angle of attack yielded a slightly higher total-pressure recovery than model A for the range of Mach number tested. An average total-pressure recovery of 0.37 was attained at a free-stream Mach number of 3.16. The total-pressure recovery of model C, obtained from both accelerating and decelerating flight, is perhaps a fairer average than that of model A where only accelerating data were obtained. Generally, the similar level of average total-pressure recovery for both cases indicates no adverse effect of a simulated angle of attack of -3°.

Although there were previously noted abrupt and erratic changes in the individual total-pressure-recovery profiles with changing Mach number, the average total-pressure-recovery data in comparison with the theoretical values indicate that the changing profiles did not change the total-pressure recovery appreciably.

[redacted]

Static-pressure ratio p/p_0 at stations 3, 5, and 6 in models A and C and at stations 1, 2, and 7 in model B are presented in figure 10 as a function of the free-stream Mach number. Generally, all static-pressure ratios at all measuring stations increased with increasing values of Mach number. The static-pressure ratios at stations 3 and 5, on the center body and outer wall in models A and C, varied abruptly at various values of free-stream Mach number, corresponding to the previously noted abrupt changes in the total-pressure profiles. Static-pressure ratios at station 6 in models A and C show higher pressure values measured on the outer wall indicated by tube b than measured on the inner-body wall by tube a over the entire Mach number range.

Static pressure at station 1 in model B could be used to check further whether the inlet was able to swallow the normal shock held outside the inlet by the contraction ratio. Comparisons with theoretical calculations show that p_1/p_0 was nearly the same as the pressure ratio behind a normal shock up to the theoretical flow-attachment Mach number of 1.88. Above this value of Mach number and up to a Mach number of 2.18, p_1/p_0 is nearly the same as the pressure ratio behind an oblique shock with a 5° corner expansion and a normal shock occurring upstream of station 1. Above $M_0 = 2.18$, p_1/p_0 lies between the theoretical pressure ratio calculated by assuming an oblique shock with a 5° corner expansion and a normal shock, and the case of an oblique shock with a 5° corner expansion and supersonic flow past the orifice at station 1. Since p_1/p_0 never approaches the value of the case of supersonic flow past the orifice at the highest Mach number reached, it is further indicated that the normal shock was never swallowed. The static-pressure ratio p_2/p_0 is slightly lower than p_1/p_0 up to $M_0 = 2.15$, as would be expected with subsonic flow past both stations 1 and 2. After $M_0 = 2.15$, values of p_2/p_0 are higher than those of p_1/p_0 up to the maximum $M_0 = 3.15$. The normal shock held in front of the inlet may meet the wedge with a lambda-shaped leg so that the measured pressure ratio p_1/p_0 may be in either a separated flow region or a supersonic area of the lambda-shaped leg. Hence, p_2/p_0 measured in a subsonic region is higher in quantity than p_1/p_0 above a free-stream Mach number of 2.15.

SUMMARY OF RESULTS

Flight tests utilizing the rocket-model technique of determining the total-pressure recovery of a two-dimensional split-wing ram-jet inlet at 0° and a simulated angle of attack of -3° with a fixed area exit

[redacted]

20 percent larger than the inlet throat yielded the following general results over a Mach number range from 1.4 to 3.16:

1. Total-pressure-recovery measurements at the diffuser exit station indicated abrupt pressure changes in the total-pressure profile throughout the Mach number range, and resulted in a wake region behind the center body wedge or outer wall.

2. A total-pressure recovery of 0.33 was obtained at a free-stream Mach number of 3.12 for 0° angle of attack. A test of a model simulating an angle of attack of -3° indicated a total-pressure recovery of 0.37 at a Mach number of 3.16.

3. Comparisons of average total-pressure recovery with the theoretical total-pressure recovery showed good agreement over the range of free-stream Mach number tested. The preliminary nature of the test does not allow a conclusion concerning the maximum total-pressure recovery that this inlet could attain.

Langley Aeronautical Laboratory,
National Advisory Committee for Aeronautics,
Langley Field, Va., February 19, 1954.

Arthur H. Hinners, Jr.
Aeronautical Research Scientist

Approved:
for Joseph A. Shortal
Chief of Pilotless Aircraft Research Division

mhg

[redacted]

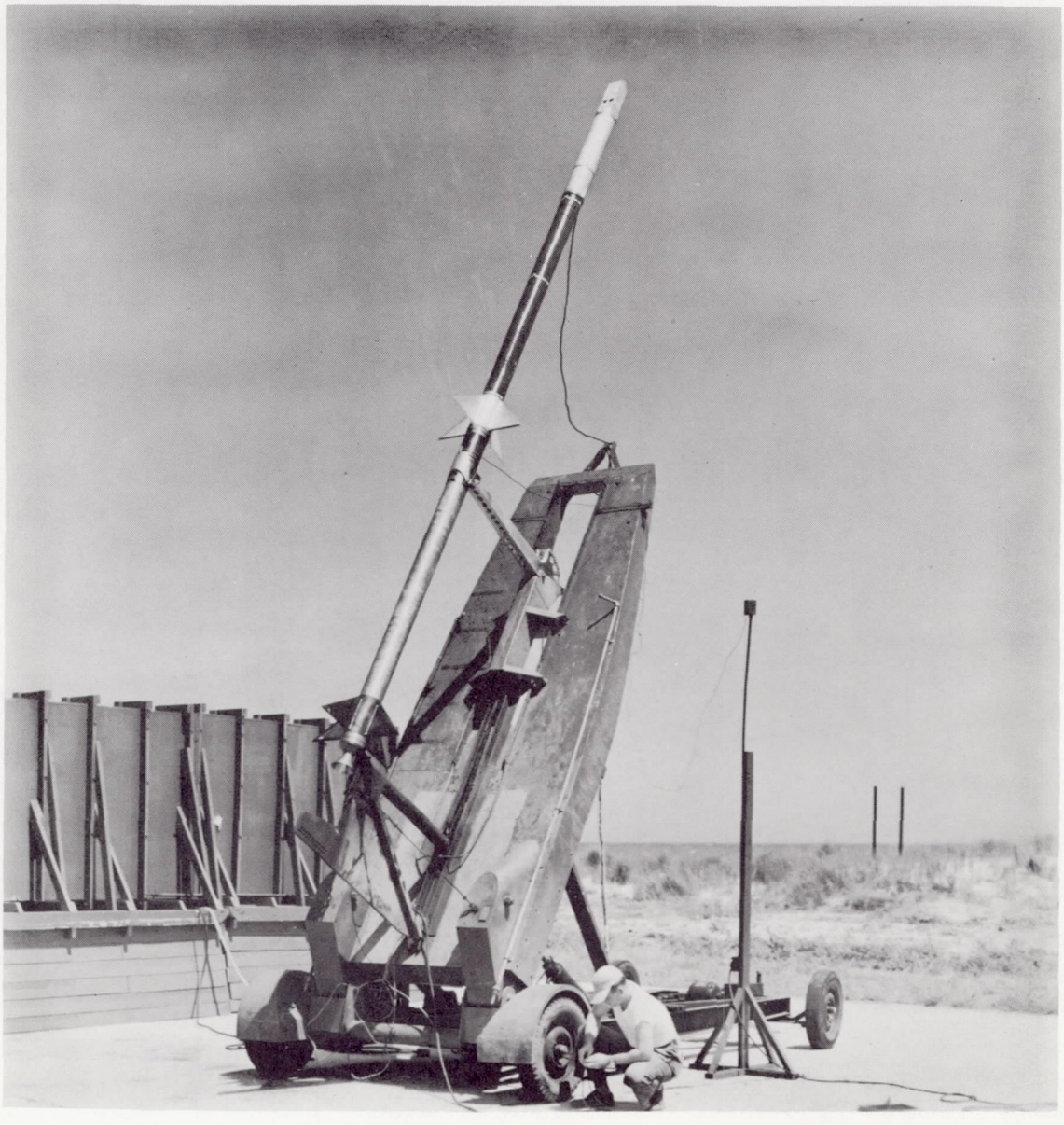

L-76326

Figure 1.- Flight test vehicle and booster rocket in launching attitude of 60°.

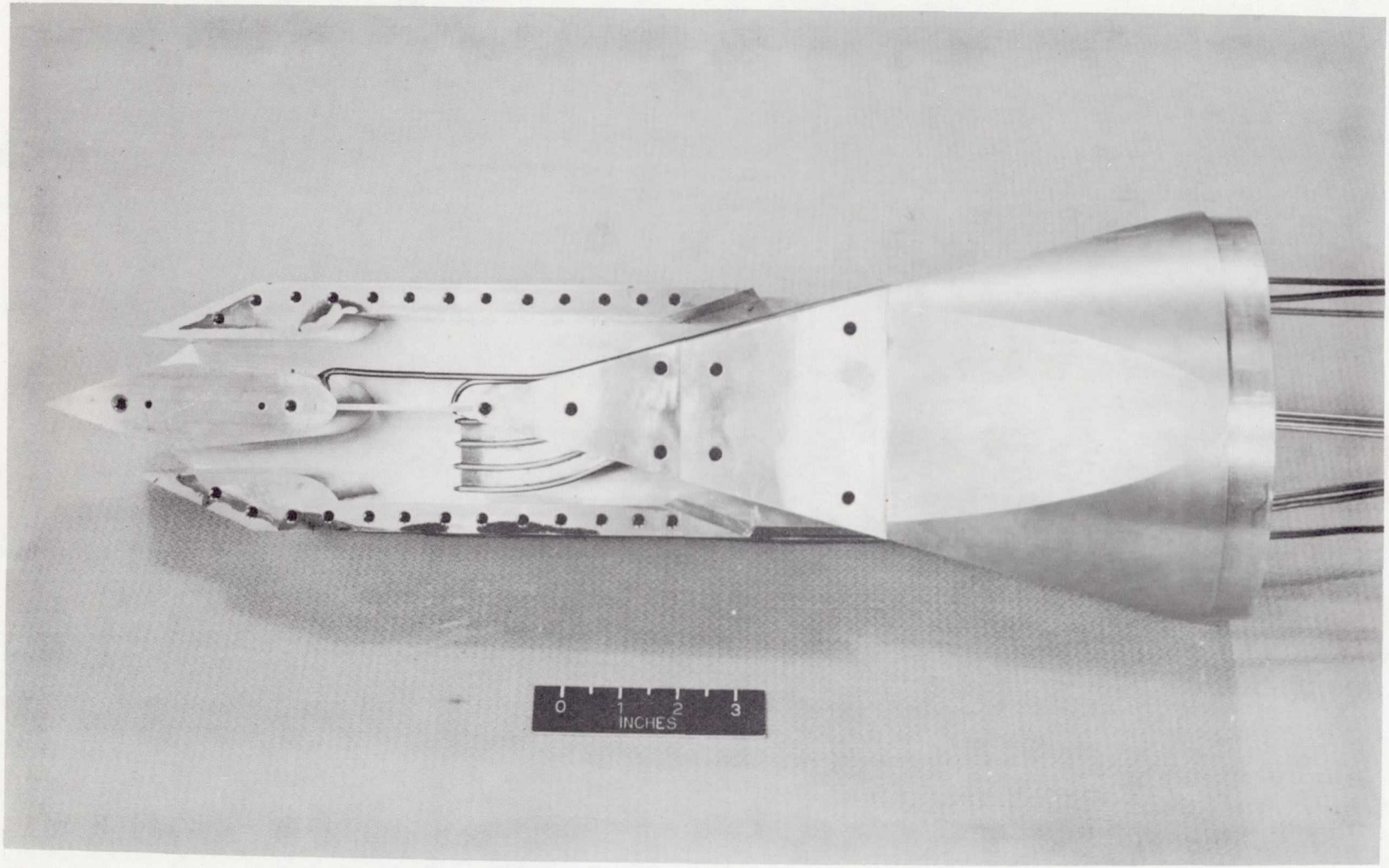

L-65662

(a) Model A with top plate removed.

Figure 2.- Two-dimensional ram-jet inlet models.

L-74034.1

(b) Models C and B, respectively, with top plates removed.

Figure 2.- Concluded.

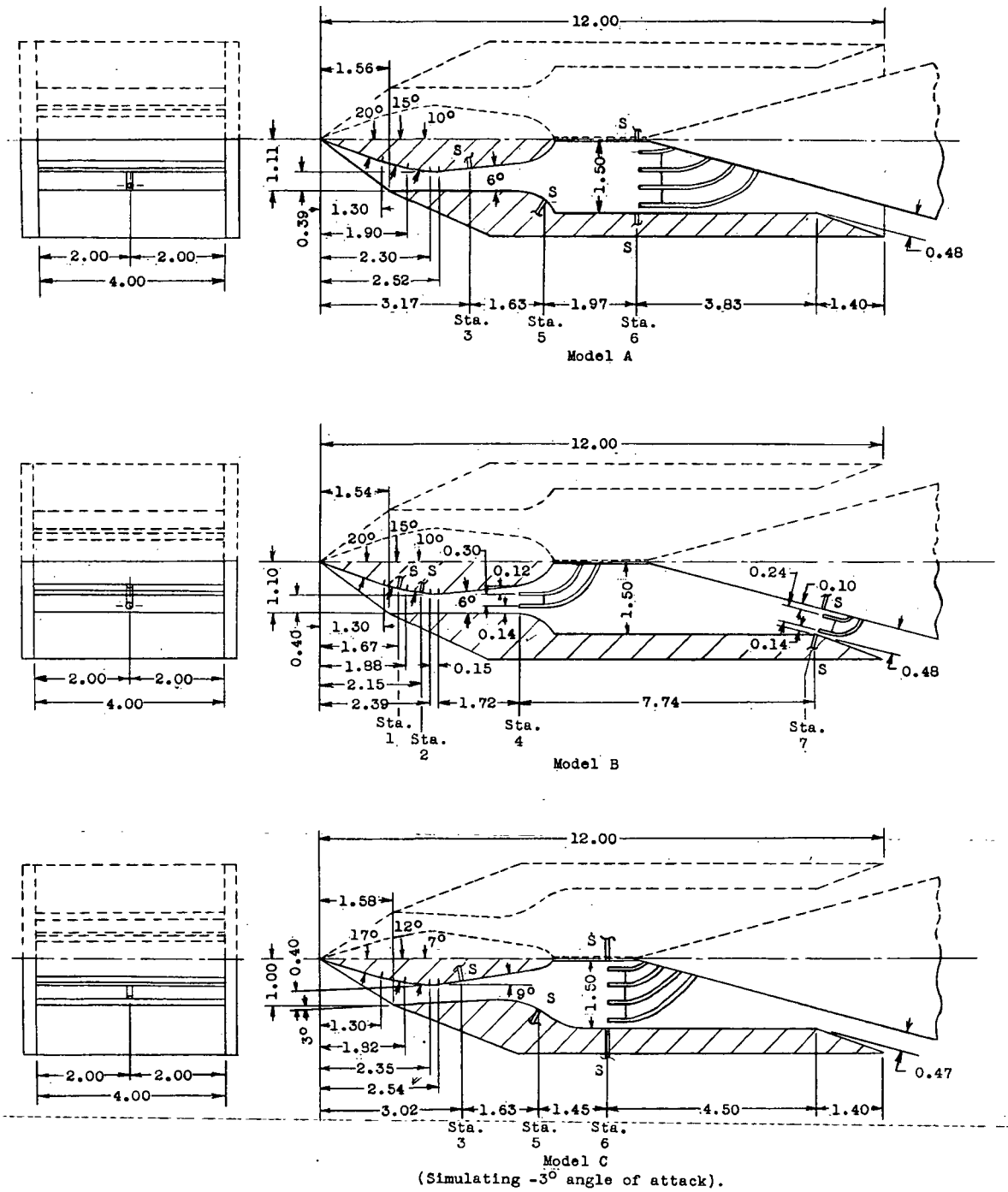

Figure 3.- Detailed diagram of models tested. All dimensions are in inches.

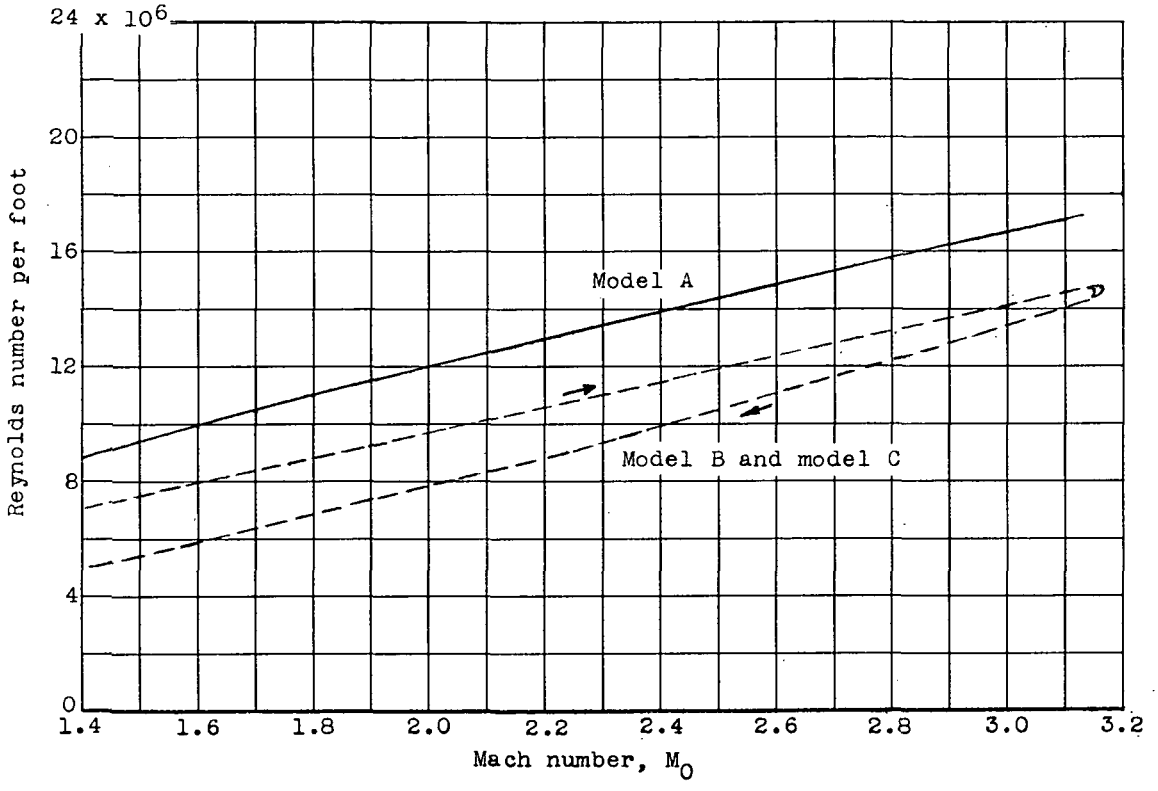

Figure 4.- Reynolds number per foot as a function of free-stream Mach number.

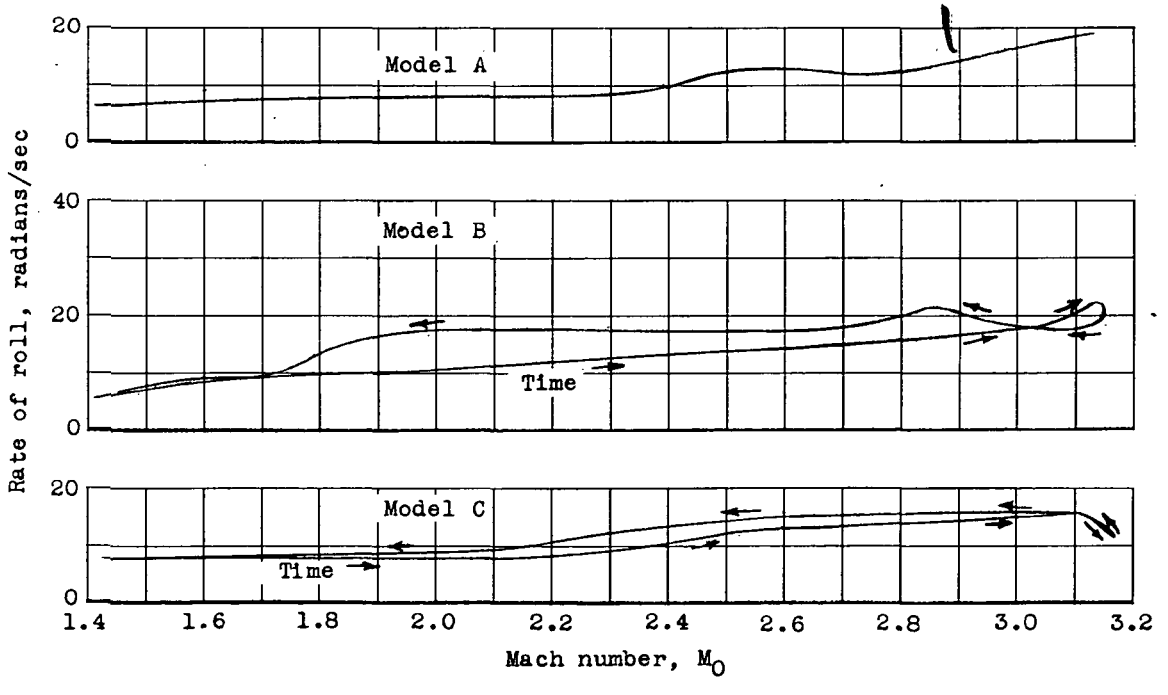

Figure 5.- Rate of roll as a function of flight Mach number.

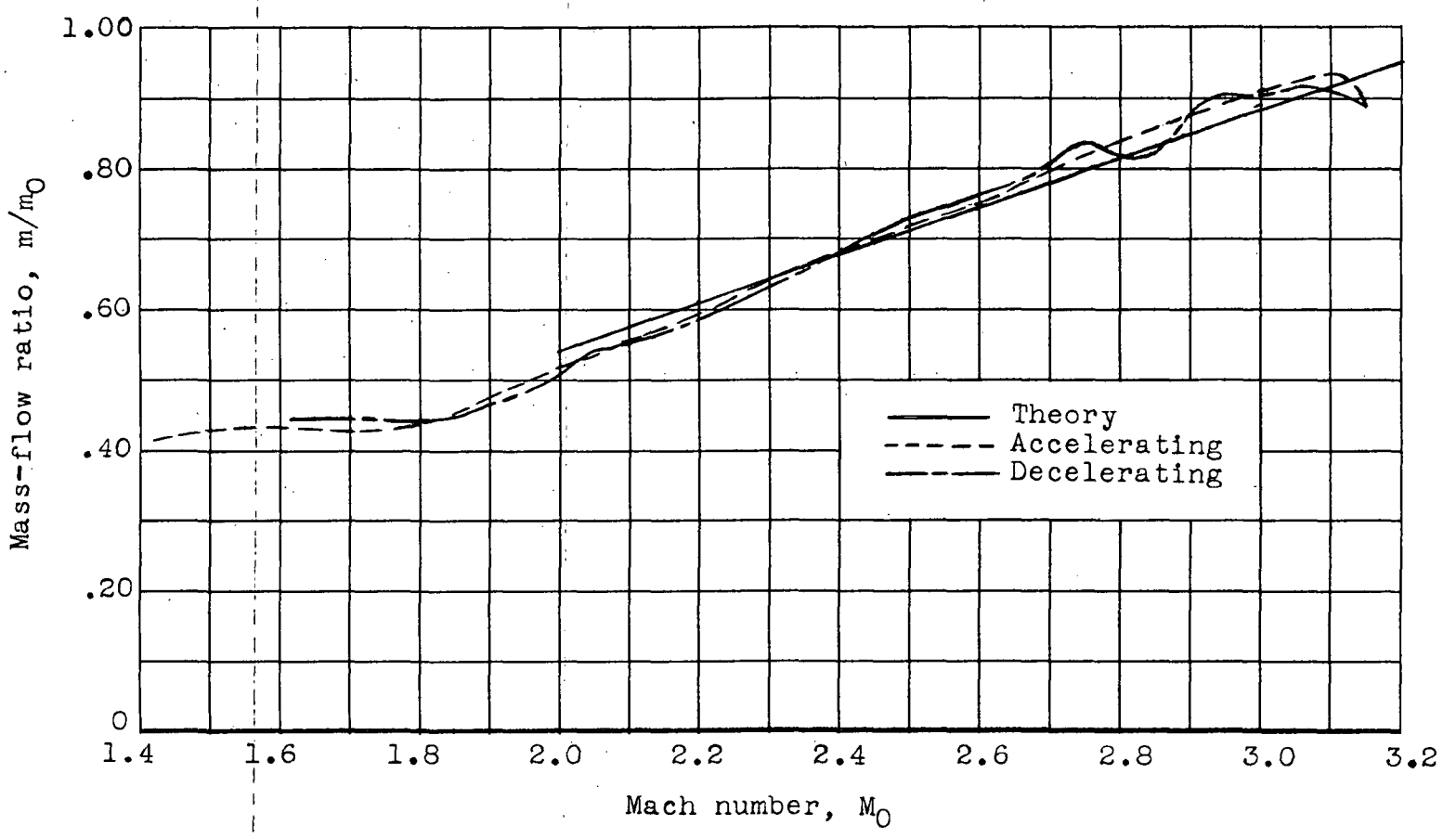

Figure 6.- Mass-flow ratio of model B as a function of free-stream Mach number.

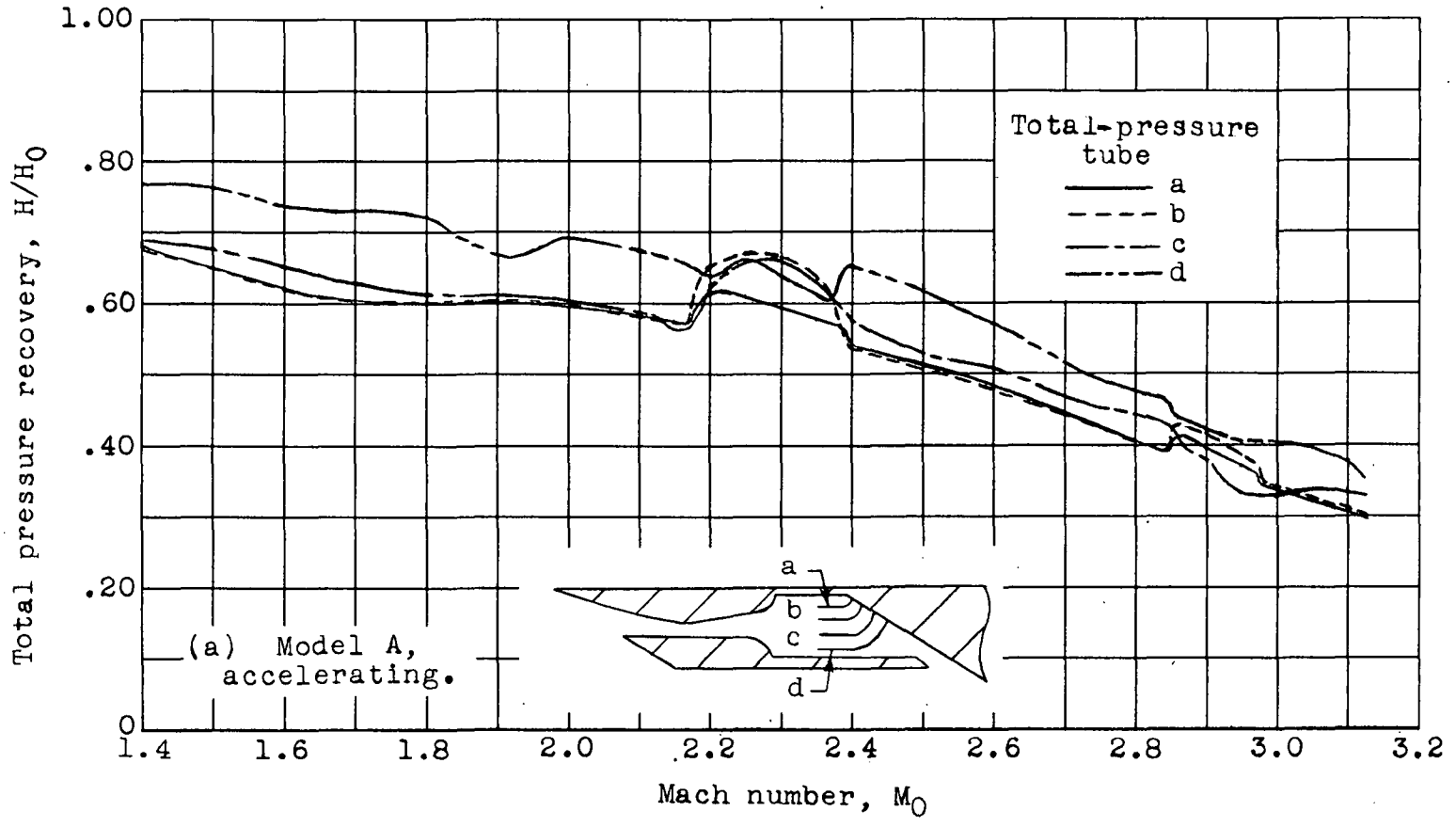

Figure 7.- Local total-pressure recovery at various total-pressure measuring stations as a function of free-stream Mach number.

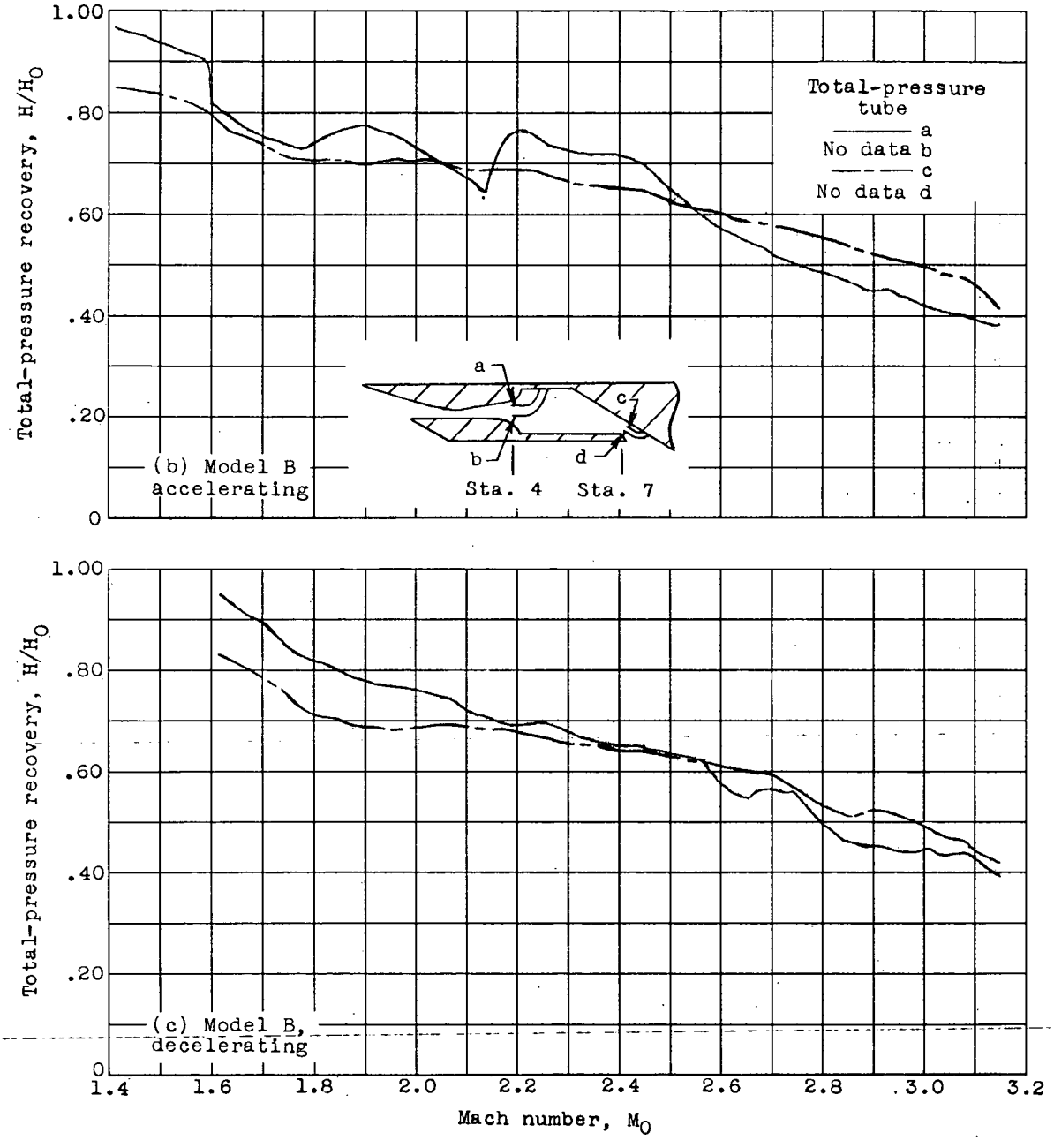

Figure 7.- Continued.

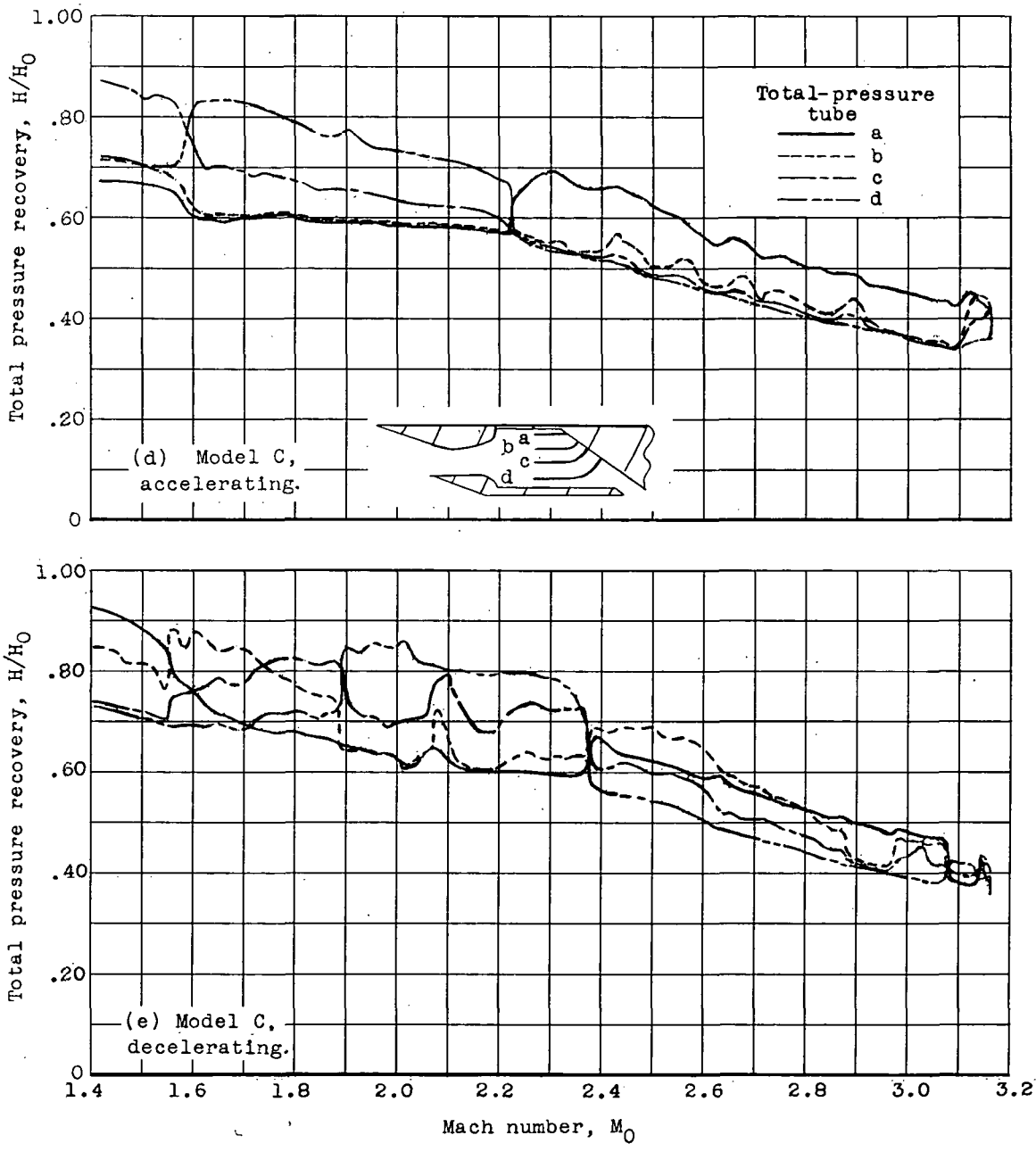

Figure 7.- Concluded.

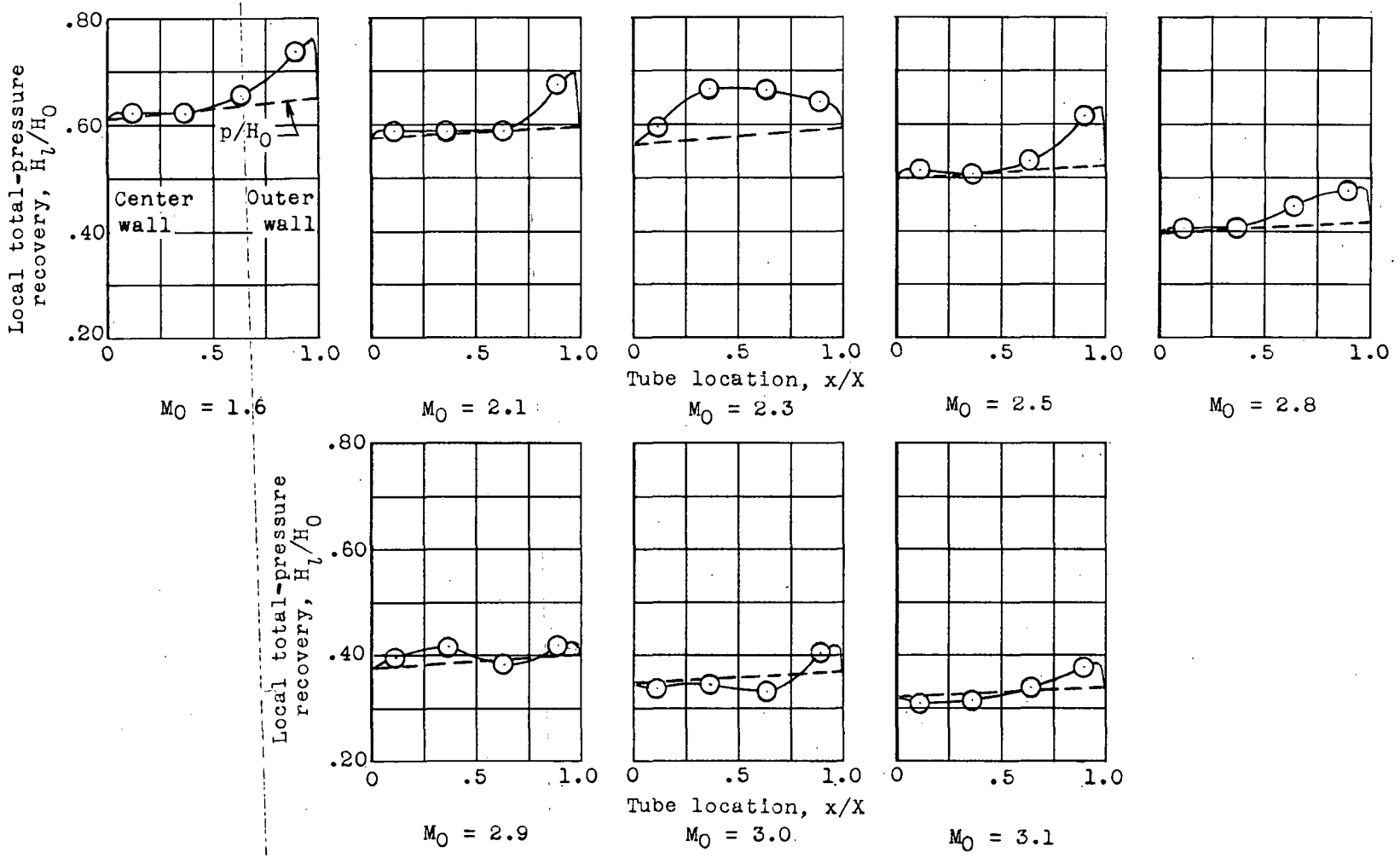

(a) Model A, station 6, accelerating data.

Figure 8.- Local total-pressure-recovery profiles at various free-stream Mach numbers.

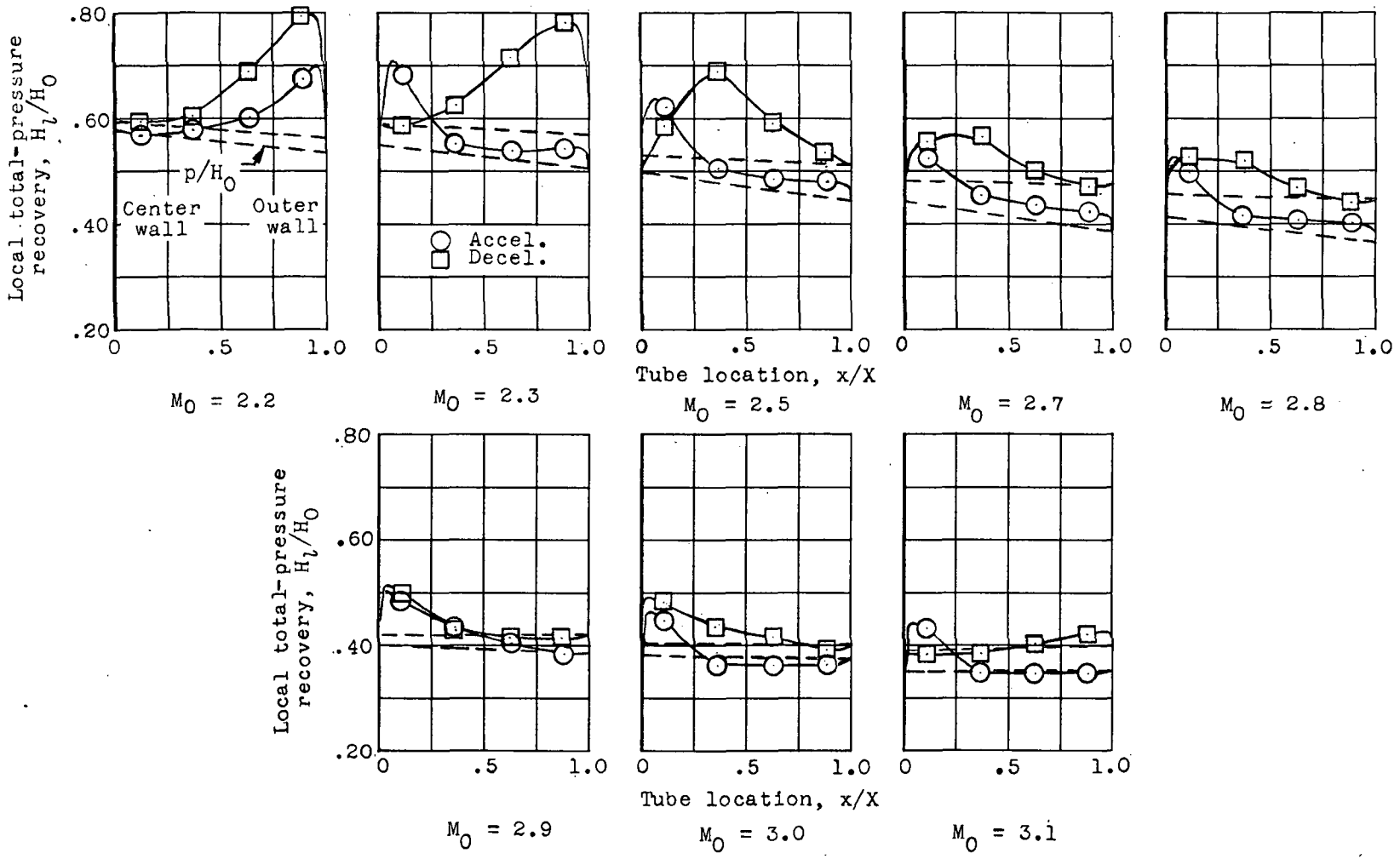

(b) Model C, station 6.

Figure 8.- Concluded.

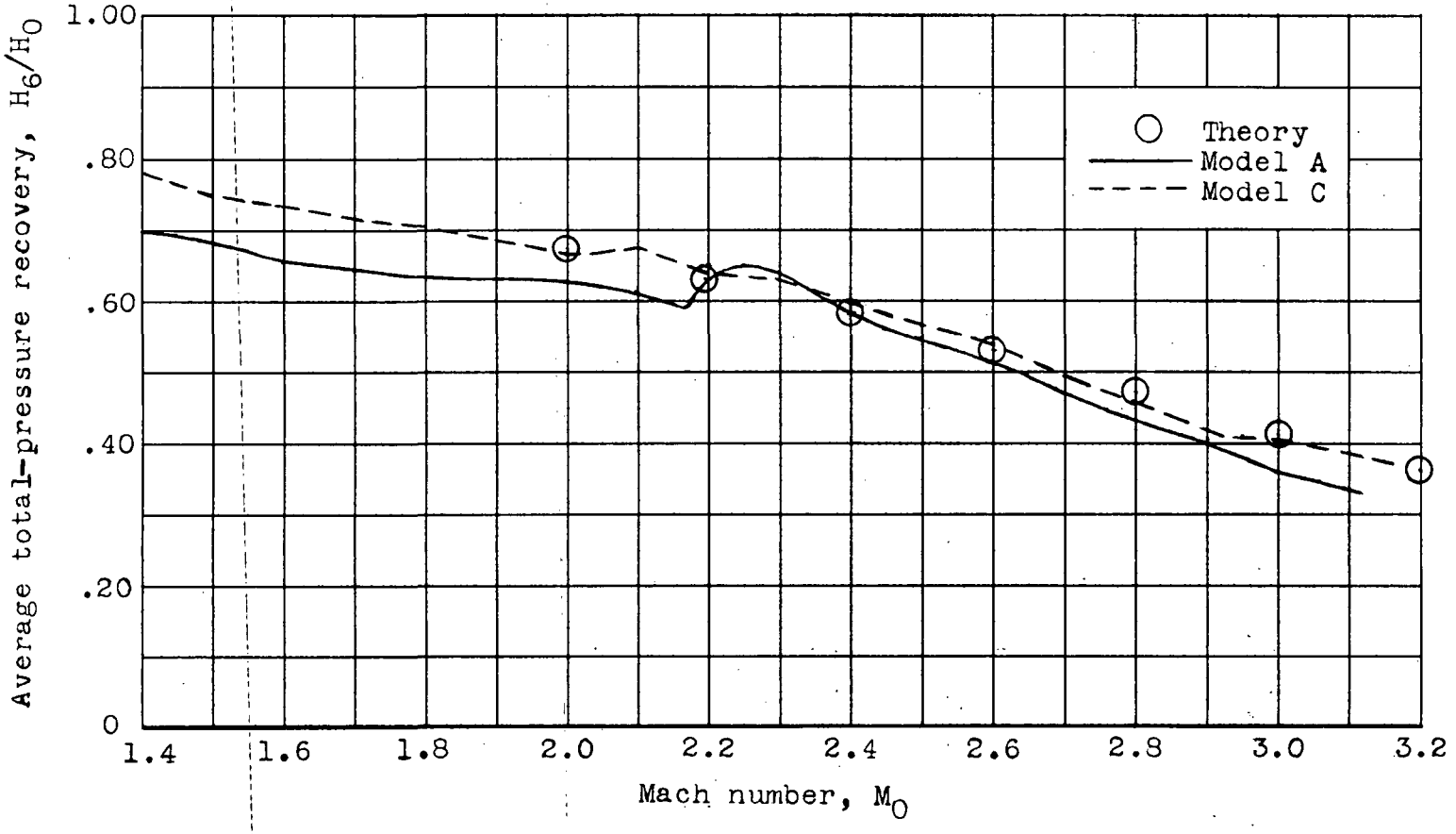

Figure 9.- Average total-pressure recovery as a function of free-stream Mach number.

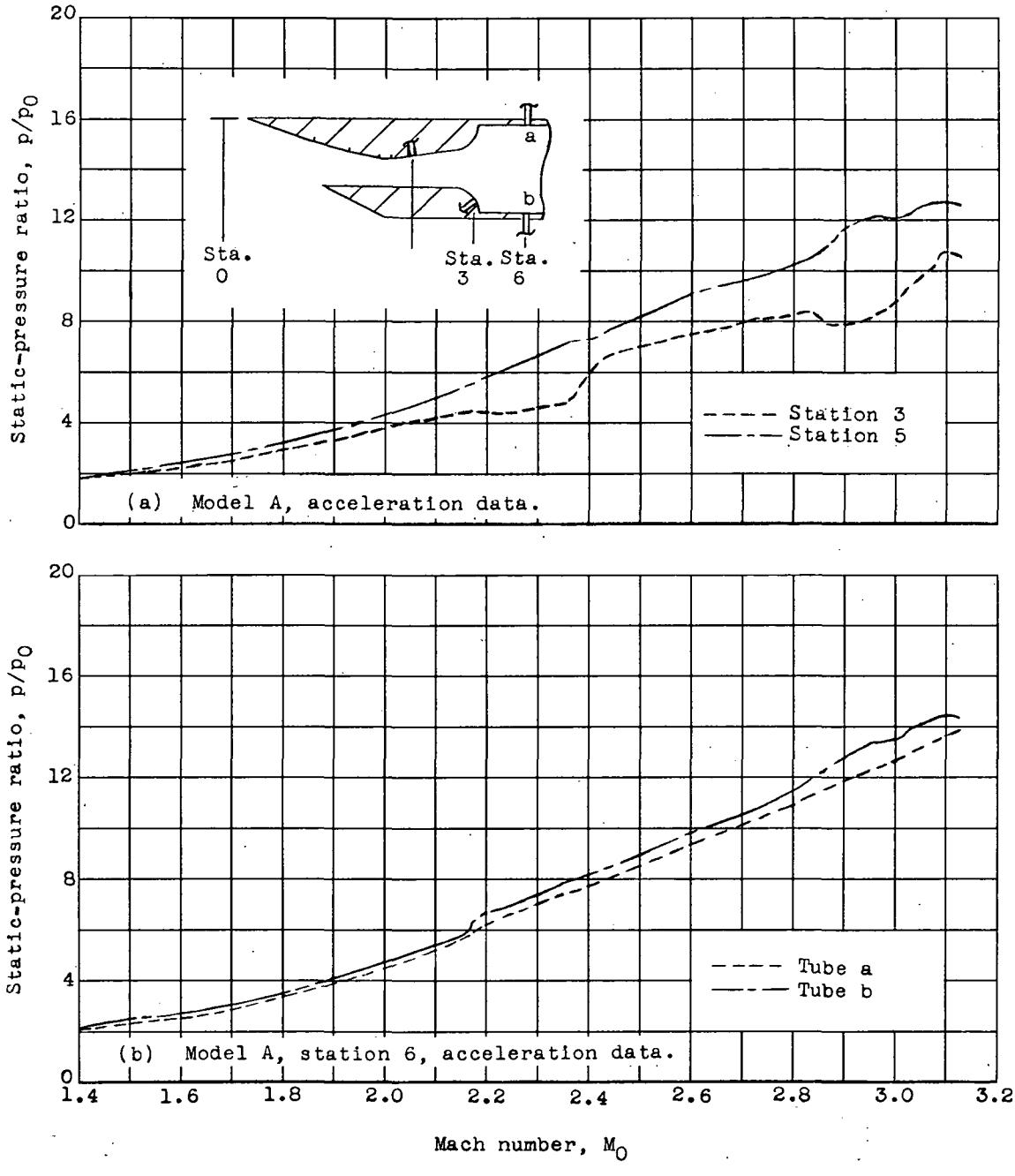

Figure 10.- Static-pressure ratio at various internal-flow stations as a function of free-stream Mach number.

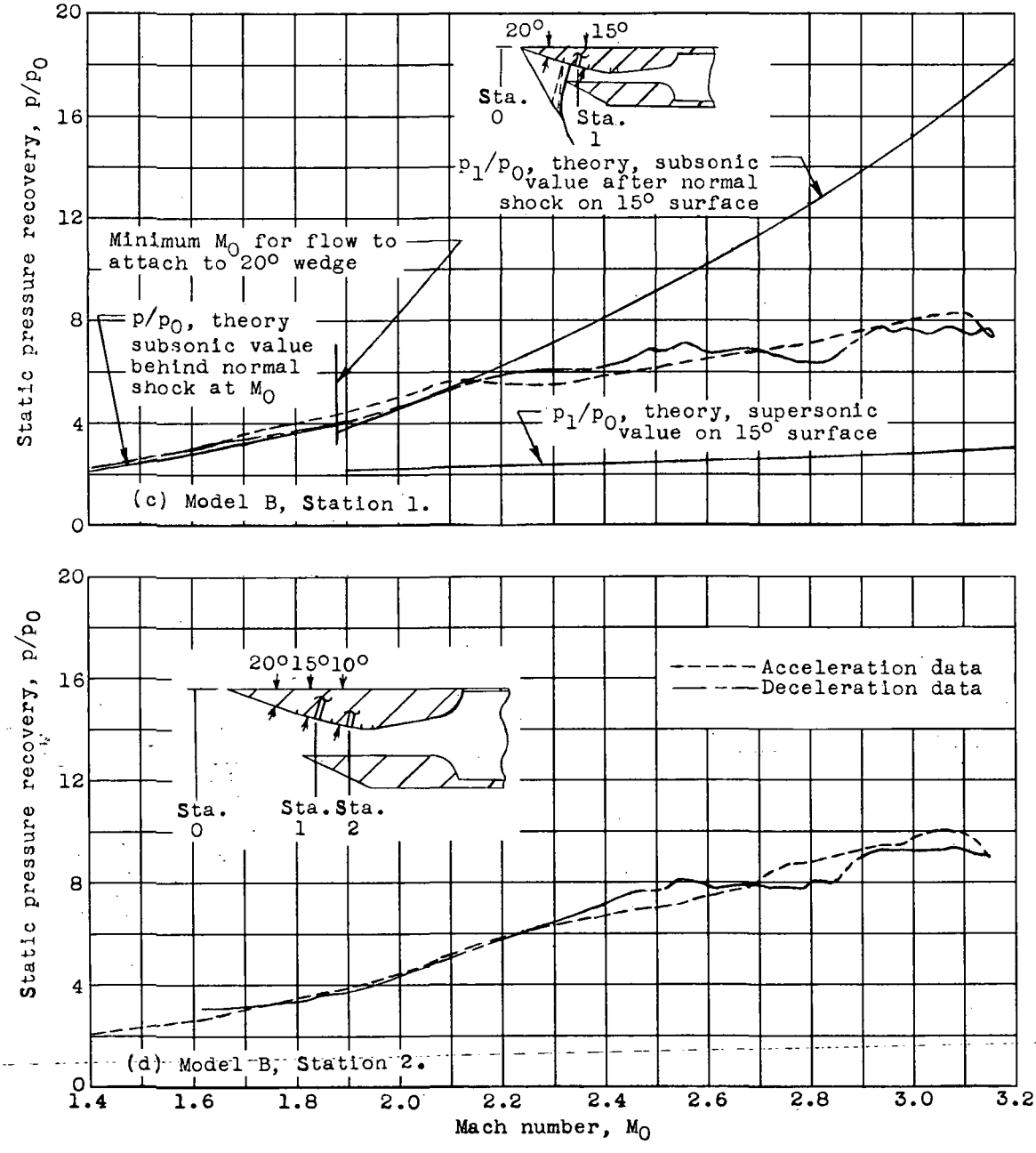

Figure 10.- Continued.

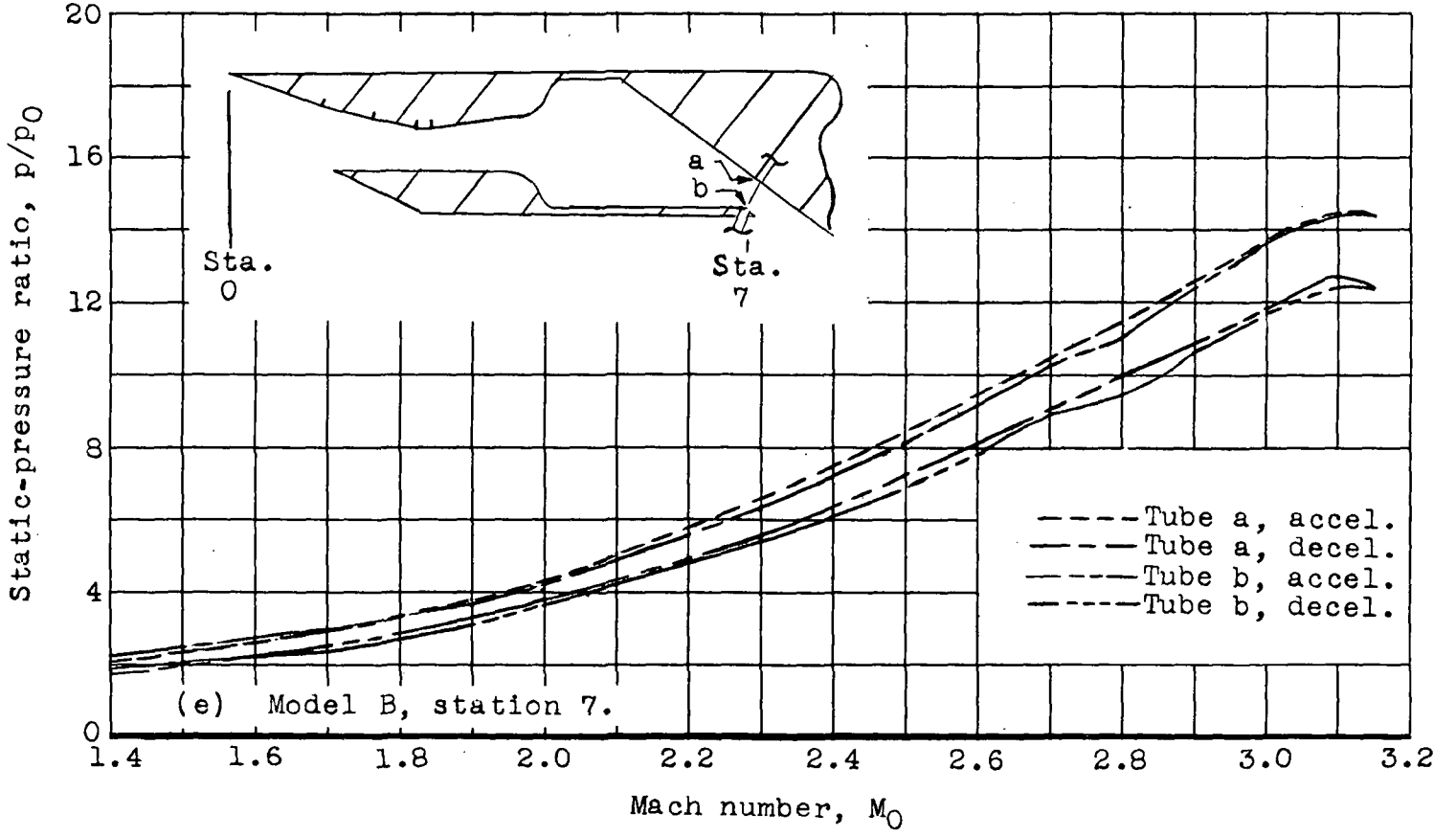

Figure 10.- Continued.

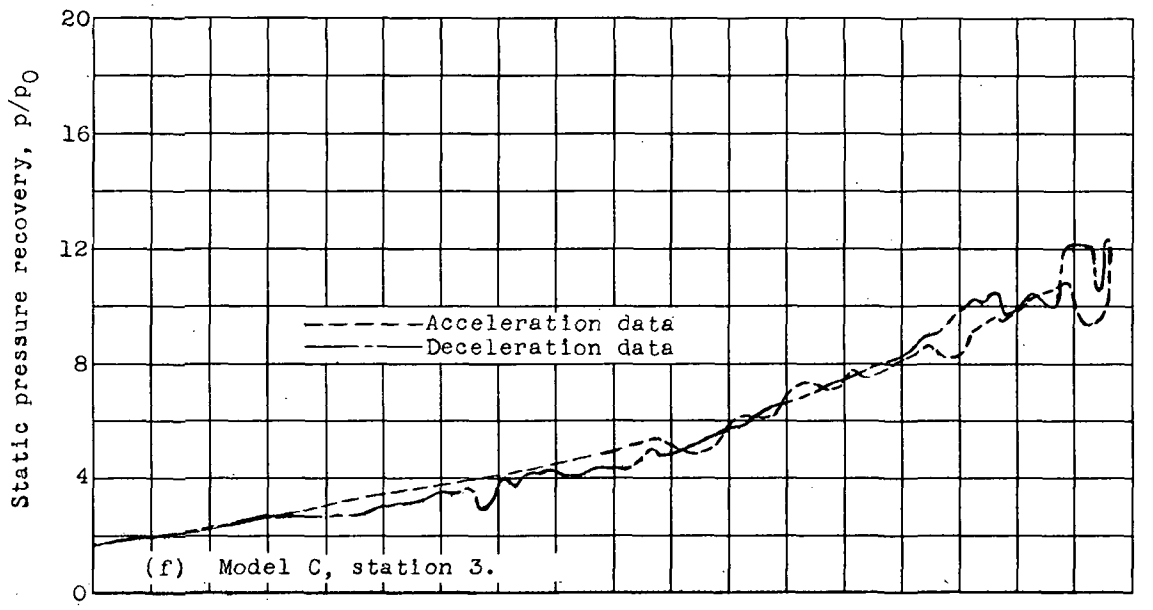

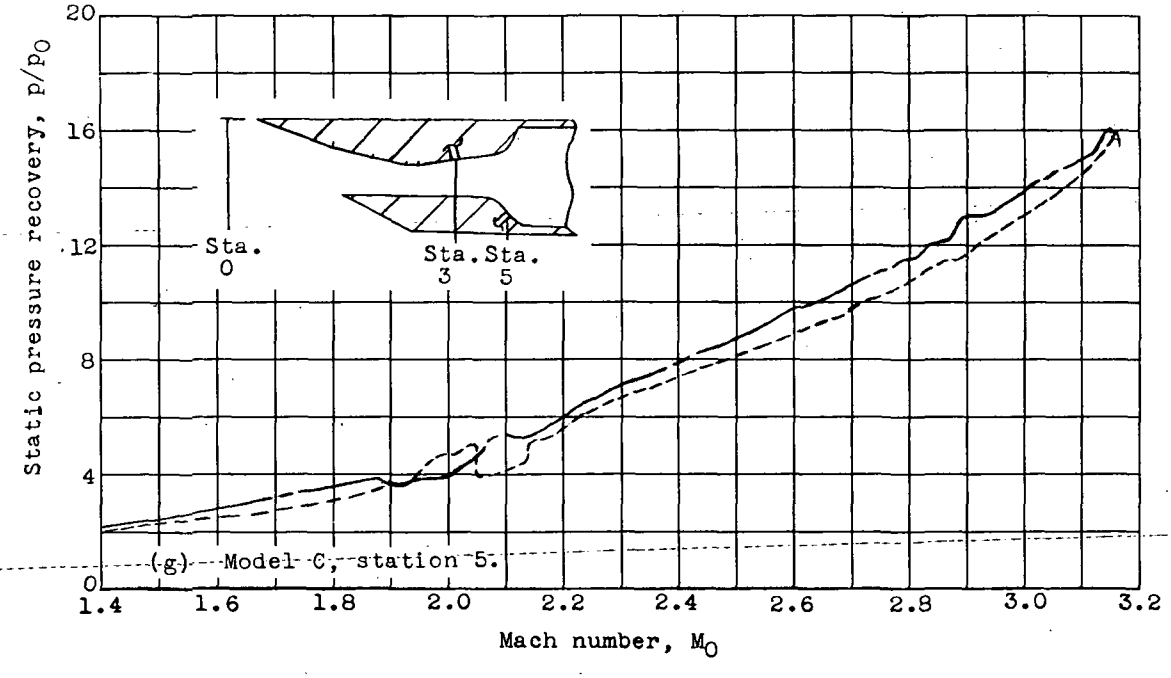

Figure 10.- Continued.

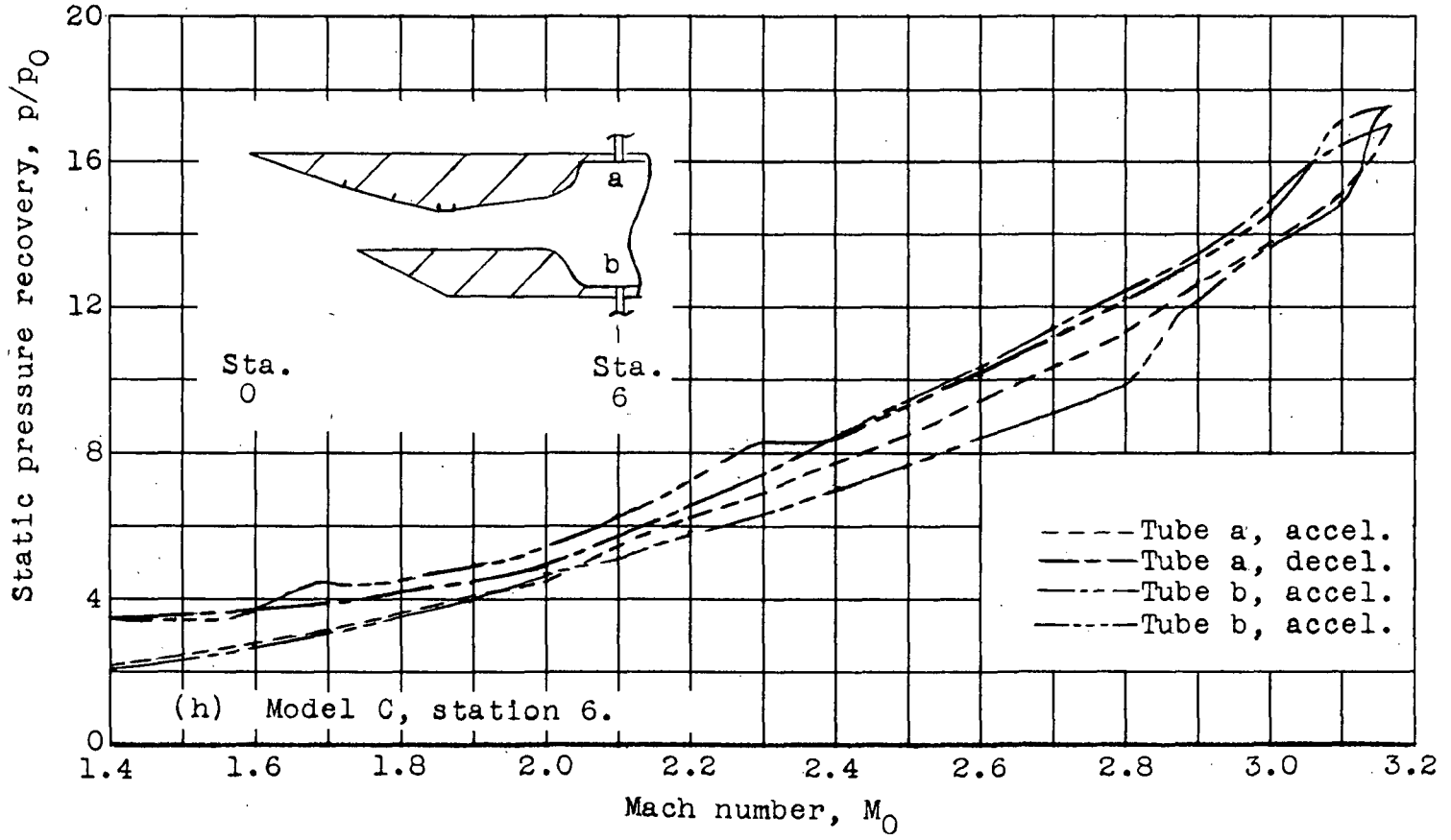

Figure 10.- Concluded.